JOURNAL OF GEOPHYSICAL RESEARCH, VOL. 102, NO. A7, PAGES 14,563–14,579, JULY 1, 1997

Ionospheric convection during nonsteady interplanetary magnetic field conditions

A.J. Ridley[1] and Gang Lu
High Altitude Observatory, National Center for Atmospheric Research, Boulder, Colorado

C.R. Clauer and V.O. Papitashvili
Space Physics Research Laboratory, University of Michigan, Ann Arbor

Abstract. We investigate six cases in which the interplanetary magnetic field (IMF) orientation is changing. The assimilative mapping of ionospheric electrodynamics (AMIE) technique is used to compute the ionospheric electric potential in a 5-min time step over the nonsteady periods. For each period a steady convection pattern prior to the convection change is determined, and this pattern is then subtracted from each of the nonsteady convection patterns. From these residual potential patterns a number of parameters can be determined, such as the start and end time of the convection change, the amount of change and the location of the strongest changes. By further examining the residual patterns, we reach the following conclusions: (1) convection changes occur in a fixed region of space, while the magnitude of the convection change grows linearly with time; (2) the strength of the convection change and the rate of the change are linearly proportional to the change observed in the IMF B_y and B_z components; and (3) the merging region may not react to long duration changes in the IMF until the ratio of $B_z/|B_y|$ passes through some threshold value. This can cause the ionospheric reconfiguration time to be less than the IMF reorientation time.

Introduction

The interplanetary magnetic field (IMF) has been shown to be strongly coupled to the magnetosphere of the Earth through magnetic merging (as first proposed by [*Dungey*, 1961]). The merging process allows the electric field of the solar wind to be applied across magnetospheric field lines. This electric field maps down to the polar ionosphere and causes the plasma to convect. By studying the ionospheric convection, a better understanding of the coupling process between the IMF and the magnetosphere can be developed.

There exist numerous theoretical and empirical models to describe the high-latitude ionospheric convection during steady IMF conditions. Most such models are based on statistical studies of electric field measurements. For example, *Rich and Hairston* [1994] used DMSP F8 and F9 drift meter measurements from September 1987 to December 1990 to find average convection patterns for different IMF conditions. Other statistical models include those by *Foster* [1983], *Heelis* [1984], *Heppner and Maynard* [1987], *Holt et al.* [1987], *Senior et al.* [1990], *Weimer* [1995], and *Ruohoniemi and Greenwald* [1996].

Another type of ionospheric convection modeling technique is based on studies which have shown that ground magnetic perturbations are linearly controlled by the IMF B_y and B_z components [*Friis-Christensen and Wilhjelm*, 1975; *Maezawa*, 1976; *Levitin et al.*, 1982; *Feldstein and Levitin*, 1986]. A regression analysis is done to data obtained from an array of magnetometer stations, and linear coefficients are determined for a grid of longitude and latitude. These coefficients, along with a model of ionospheric conductivity, can then be used to determine the ionospheric potential for any IMF orientation. The Izmiran electrodynamic model (IZMEM) [*Belov et al.*, 1977; *Papitashvili et al.*, 1994] and the model presented by *Friis-Christensen et al.* [1985] are two examples of this technique.

The assimilative mapping of ionospheric electrodynamics (AMIE) technique [*Richmond and Kamide*, 1988] has been used in a number of studies of ionospheric phenomena [e.g., *Knipp et al.*, 1991, 1993; *Lu et al.*, 1994]. Unlike most ionospheric convection models, AMIE utilizes simultaneous data to compute global ionospheric electric fields. The different data sets are combined to make a "snapshot" map of the ionospheric electric field by inverting all of the data which are gathered for the time period under investigation. The AMIE technique combines all available data within a user-defined time window and produces a convection pattern for that time period. Since the time window is flexible, depending on the time resolution of the input data as well as the geophysical phenomenon of interest, the AMIE technique

[1] Also at Space Physics Research Laboratory, University of Michigan, Ann Arbor.

Paper number 97JA00940.
0148-0227/97/97JA-00940$09.00

is a suitable tool to study both steady state and time-varying phenomena.

Most of the above models show similar features in the large-scale convection of the polar cap ionosphere for a given steady IMF orientation. When the IMF is directed southward (B_z negative), the flow over the polar region is directed antisunward, with the return (sunward) flow at lower latitudes. When the IMF is directed strongly northward (B_z positive and greater than the magnitude of B_y), most models show that the flow over the summer pole is reversed (i.e., directed sunward over the pole and antisunward at lower latitudes) and is confined to a small region of the polar cap. These models also show the effect of B_y on the polar cap convection. When B_y is positive (and B_z is negative or slightly positive), it is observed that the dusk (morning) cell in the northern (southern) hemisphere becomes large and round, while the dawn (afternoon) cell becomes elongated and narrow. The opposite is true when B_y is negative.

The nonsteady aspects of the high-latitude convection have been of interest also. Past studies have been done to describe the amount of time the ionospheric convection takes to change from one steady pattern to another steady pattern, after sudden changes in the IMF or solar wind [e.g., *Hairston and Heelis*, 1995]. These studies do not attempt to explain how the convection changes, but describe only the amount of time needed for the convection pattern to change after certain IMF orientation changes.

Recently, studies have begun focusing on describing how the convection in the polar cap changes as the IMF changes [*Etemadi et al.*, 1988; *Clauer and Friis-Christensen*, 1988; *Greenwald et al.*, 1990; *Lockwood et al.*, 1990; *Lester et al.*, 1993; *Ridley and Clauer*, 1996]. For example, *Saunders et al.* [1992] showed an example of an oscillating IMF B_z. Simultaneous with the B_z oscillations, ground-based magnetometers measured oscillations in the north-south component of the magnetic field measured at the ground. The oscillations were observed to have a longitudinal phase delay, consistent with a twin vortex forming around 1000 magnetic local time (MLT) and expanding longitudinally with a phase speed of 5 km/s.

Another study of changing convection patterns was done by *Stauning et al.* [1995], *Clauer et al.* [1995], and *Papitashvili et al.* [1995]. Theyed show an example of magnetic signatures consistent with a poleward progressing current structure. This occurred during a time period when the IMF B_y was strongly positive but modulating in strength. They hypothesized that these were perturbations in the *DPY* current structure, caused by the IMF B_y oscillations, produced at the cusp latitudes spreading poleward, causing the convection to change.

These studies show similar results, namely that when the IMF changes orientation, the convection pattern begins to change near the ionospheric projection of the cusp within a few minutes of when the IMF change encounters the magnetopause. The ionospheric reconfiguration is then spread out through the rest of the ionosphere, over a period of 5-20 min. A propagation of the new ionospheric convection pattern away from the ionospheric projection of the cusp can be observed, and a velocity can be measured.

Most studies of changing ionospheric convection use localized observations. The two studies discussed above use magnetometer chains which span a limited region of latitude and magnetic local time (MLT). Other studies

Table 1. A List of the Stations Used

Station ID	Apex Latitude	Apex Longitude	Network or Provider
ALT	66.65	107.08	IMAGE
AMS	49.04	138.35	NGDC
AMU	60.94	-96.65	NGDC
ATU	74.91	39.26	Greenland
AVI	68.47	-99.22	NGDC
BAC	68.30	-28.92	CANOPUS
BJO	71.43	109.11	Norway
BLC	74.34	-34.22	NGDC
BNG	5.30	57.21	NGDC
BOU	49.25	-41.12	NGDC
BRW	69.87	-110.43	NGDC
BSL	41.69	-20.19	NGDC
CBB	77.50	-53.43	NGDC
CHU	69.30	-29.02	CANOPUS
CLF	43.90	79.92	NGDC
CMO	64.99	-97.41	NGDC
CNB	45.74	-133.54	NGDC
CON	73.39	-59.31	CANOPUS
CSY	80.67	155.50	NGDC
CZT	53.20	106.29	NGDC
DAW	65.95	-89.15	CANOPUS
DLR	39.48	-34.41	Intermagnet
DNB	75.23	81.22	Greenland
DRV	80.63	-124.76	NGDC
DVS	74.65	100.31	NGDC
ESK	52.95	77.94	CANOPUS
FAR	60.95	78.28	SAMNET
FRD	49.76	-3.18	NGDC
FRN	43.22	-56.93	NGDC
FYU	67.17	-96.70	NGDC
GDH	76.13	40.77	Greenland
GHB	70.99	38.43	Greenland
GIL	66.97	-29.39	CANOPUS
GML	55.10	78.35	SAMNET
GUA	5.55	-144.59	NGDC
HAD	48.11	75.35	Intermagnet
HER	42.50	82.30	NGDC
HON	21.67	-90.74	NGDC
HOP	72.94	116.13	NORWAY
ISL	64.54	-28.96	CANOPUS
JAN	70.51	84.64	NORWAY
KAK	28.82	-148.77	NGDC
KEV	66.32	110.10	IMAGE
KIL	65.98	104.69	IMAGE
KNY	24.21	-157.63	NGDC
KVI	56.09	96.52	SAMNET
LER	58.17	81.78	Intermagnet

The first column gives the IAGA code of the magnetometer, the second and third columns give the apex latitude and longitude of the station. The last column lists the corresponding magnetometer chain (see acknowledgments for more details).

have used radars [*Clauer and Friis-Christensen*, 1988; *Etemadi et al.*, 1988; *Greenwald et al.*, 1990; *Lockwood et al.*, 1990; *Clauer et al.*, 1995] and other localized measurements such as imaging riometers [*Stauning et al.*, 1995]. With the availability of global data sets as well as the advent of data assimilation techniques, studies of convection over the entire polar region, instead of a localized region, become feasible. This allows examinations of the ionospheric response to the IMF changes in a global fashion.

AMIE Results and Analysis

The AMIE technique uses both ground and satellite observations of magnetic perturbations, plasma velocity and particle precipitation measurements to derive ionospheric conductivities and electric potential patterns. The method for calculating the electric potential from data has been discussed in a number of papers [*Richmond and Kamide*, 1988; *Knipp et al.*, 1993]. A list of the magnetometers and radars used in this study is shown in Table 1. Included in this table is the International Association of Geomagnetism and Aeronomy (IAGA) code for each station (for observatory names, see [*Abston et al.*, 1985]) with their respective apex latitude and longitudes (which, at high latitudes, are identical to corrected geomagnetic coordinates) [*Richmond*, 1995, and references within]. The ion drift and precipitating particle data were taken from the DMSP F8, F9 and F10 satellites, which are in Sun synchronous polar orbits at an altitude of about 850 km. These satellites have an orbital period of approximately 100 min. Figure 1 shows the locations of all data sources at 1200±45 min UT on May 18, 1991. The potential patterns used in this study were derived using 5-min-averaged magnetometer measurements and 6 min worth of satellite and radar measurements, within ± 3 min of a given time.

Table 1. Cont.

Station ID	Apex Latitude	Apex Longitude	Network or Provider
LNP	17.88	-167.40	NGDC
LOV	55.92	96.62	Intermagnet
LRV	65.36	67.94	NGDC
MBC	80.88	-89.25	Intermagnet
MBO	5.29	57.20	NGDC
MCM	80.05	-32.86	CANOPUS
MEA	62.30	-55.34	NGDC
MMB	36.65	-145.18	NGDC
MUO	64.77	106.08	IMAGE
NAA	76.06	112.39	Norway
NAQ	66.78	43.81	Greenland
NOR	61.60	95.67	SAMNET
NRD	80.90	106.68	Greenland
NUR	56.90	102.78	SAMNET
OTT	56.60	0.31	NGDC
OUL	61.71	106.05	SAMNET
PAF	58.42	122.12	NGDC
PEL	63.62	105.74	IMAGE
PIN	60.81	-30.45	CANOPUS
PPT	16.30	-75.24	Intermagnet
RAB	68.95	-25.70	CANOPUS
RAN	73.28	-26.79	CANOPUS
SAH	76.33	-84.67	NGDC
SCO	71.87	73.83	Greenland
SIM	67.61	-68.89	CANOPUS
SJG	29.12	9.44	NGDC
SKT	72.41	37.89	Greenland
SMI	67.85	-56.16	CANOPUS
SOD	63.96	108.07	Intermagnet
SOR	67.36	107.12	IMAGE
STF	73.53	41.93	Greenland
STJ	54.52	31.03	NGDC
THL	85.64	34.87	Greenland
THY	42.03	92.89	Intermagnet
TIK	65.78	-163.07	NGDC
TLK	61.97	-97.50	NGDC
TRO	66.70	103.87	Norway
TUC	40.01	-46.07	NGDC
UPN	79.76	42.67	Greenland
VIC	54.01	-64.71	NGDC
YOR	51.15	79.12	SAMNET
Sondrestrom	73.53	41.93	SRI
Goose Bay	61.92	22.96	JHU/APL

The final two entries are the radars used in the study.

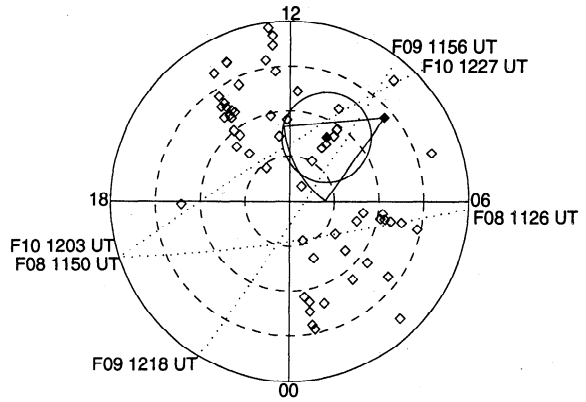

Figure 1. Locations of magnetometers, radars and satellites above 50° apex latitude for 1200 UT on May 18, 1991. The magnetometers are displayed as open diamonds. The location of the Sondrestrom and Goose Bay radars are indicated by solid diamonds, with their fields of view shown as a circle and a pie wedge, respectively. The DMSP flight paths are shown as dotted lines, with the starting and stopping times of the satellite pass indicated.

We have used the AMIE technique to study three intervals in which the IMF and solar wind were nonsteady. In two of the three intervals, the IMF underwent an orientation change, while the solar wind parameters remained roughly constant. During the third interval, the solar wind plasma density decreased significantly, while the total strength of the IMF grew.

May 18, 1991

Figure 2 shows the IMF and solar wind conditions for the first event: 1030-1300 UT on May 18, 1991. The solar wind speed and plasma density are of typical values during the interval 1040-1140 UT; no data exist

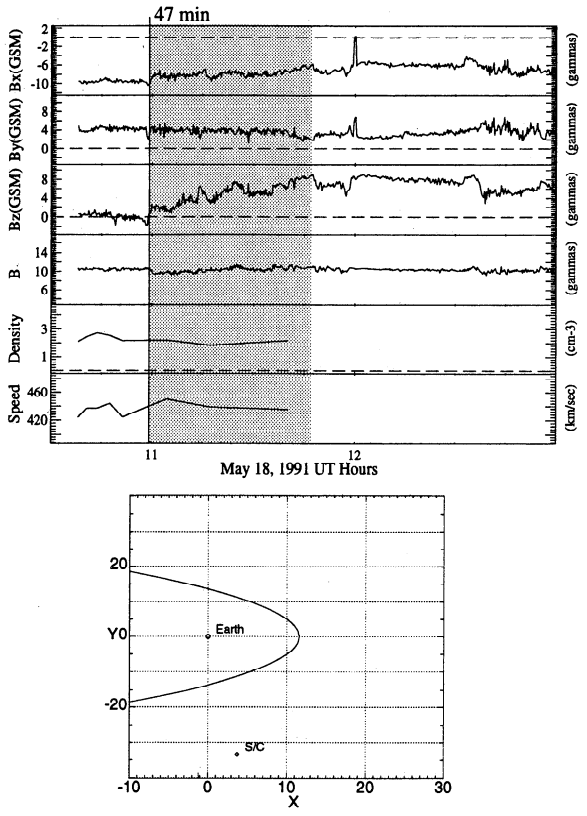

Figure 2. Interplanetary magnetic field (IMF), plasma number density and speed measurements from the IMP 8 satellite. The plots are, from top to bottom, B_x, B_y, B_z, the magnitude of the IMF, the number density of the solar wind plasma and the flow speed of the plasma. The vertical line at 1059 UT indicates the start of the IMF orientation change, while the shaded region is the time interval in which the IMF is changing. The small diagram below shows the location of the IMP 8 spacecraft (S/C) with respect to the Earth and the magnetosphere in the GSE X-Y plane.

for subsequent time periods. There are no IMF data before 1040 UT, but convection patterns derived from AMIE indicate that the IMF is steady prior to this time. At 1100 UT, the IMF B_z begins to increase from 0 nT to 8 nT. This change is approximately linear and takes about 45 min. During this interval, both B_x and B_y remain constant at -8 nT and 4 nT, respectively.

Figure 3 shows the electric potentials derived by the AMIE technique for the time interval 1040 - 1120 UT. The convection patterns from 1040 - 1055 UT are very similar and show a clear B_y positive dominated convection pattern, where the morning cell is elongated and wrapped around the circular afternoon cell.

At 1105 UT the convection starts to change dramatically. Convection cells are observed to move, and seemingly break other cells apart. When the convection pattern settles down, by approximately 1130 UT, there is a distinctive three-cell convection pattern. The two central cells are reversed convection cells similar to those discussed in a variety of papers [e.g., *Reiff*, 1982; *Clauer and Friis-Christensen*, 1988; *Crooker*, 1992; *Cannon et al.*, 1992]. The third cell (on the night side) is similar to the one obtained from IZMEM [see *Papitashvili et al.*, 1994, Figure 5] associated with B_z positive convection. This cell is most likely caused by viscous interaction between the solar wind and the magnetosphere. The sequence of the ionospheric convection change is very similar to the one observed by *Knipp et al.* [1991].

The small size of the convection pattern, along with the sparse number of data points above 80° latitude, implies that the convection pattern (after 1105 UT) may be misrepresented. One of the important features of the AMIE technique is the ability to estimate quantitatively the uncertainty in the fitted patterns. The uncertainty at a point is related to how close that point is to a data point. The change in the uncertainty as the distance from a data point increases is related to the spatial size and magnitude of the potential pattern. Because of the sparse data coverage between 1700 and 2300 MLT, the convection pattern in that region is determined from the extrapolation of the nearby data points. In this region the uncertainty in the large-scale electric field is greater than 50%. In all other regions the uncertainty is less than 50%. This includes all of the dawnside negative potential cell and most of the duskside positive potential cell. At approximately 1140 and 1210-1220 UT the DMSP satellites flew close to the reversed convection cells (as indicated in Figure 1). Convection data from the DMSP satellites provide strong constraints for the AMIE inversion. The shape and size of the convection pattern do not change significantly during the interval having DMSP data. Therefore, we feel very confident that the strongest convection cells are being represented accurately.

To further our investigation of the changes in convection configuration, a base potential pattern is subtracted from the potential patterns. The residual patterns thus obtained illustrate more clearly the relative variations. To ensure that the steady pattern does not contain any small-scale, localized features (which may corrupt the residual potential patterns), a number of steady patterns are averaged together. For this first convection change, the patterns from 1040 - 1055 UT are averaged and used as the steady (base) convection pattern. This average pattern is shown in Figure 4a.

The residual patterns are shown in Figure 4b. The contours show the potential difference between the current and base pattern. The solid contours represent an increase in potential, while the dashed contours represent a potential decrease. For the first pattern there is simply random noise, since this is one of the averaged patterns for the base pattern. The next few patterns show a two-cell convection pattern, with the centers close to the dawn - dusk meridian at approximately 84° invariant latitude.

It is observed that the residual convection pattern resembles a reversed two-cell convection pattern, although there is an asymmetry to the twin vortex structure, with

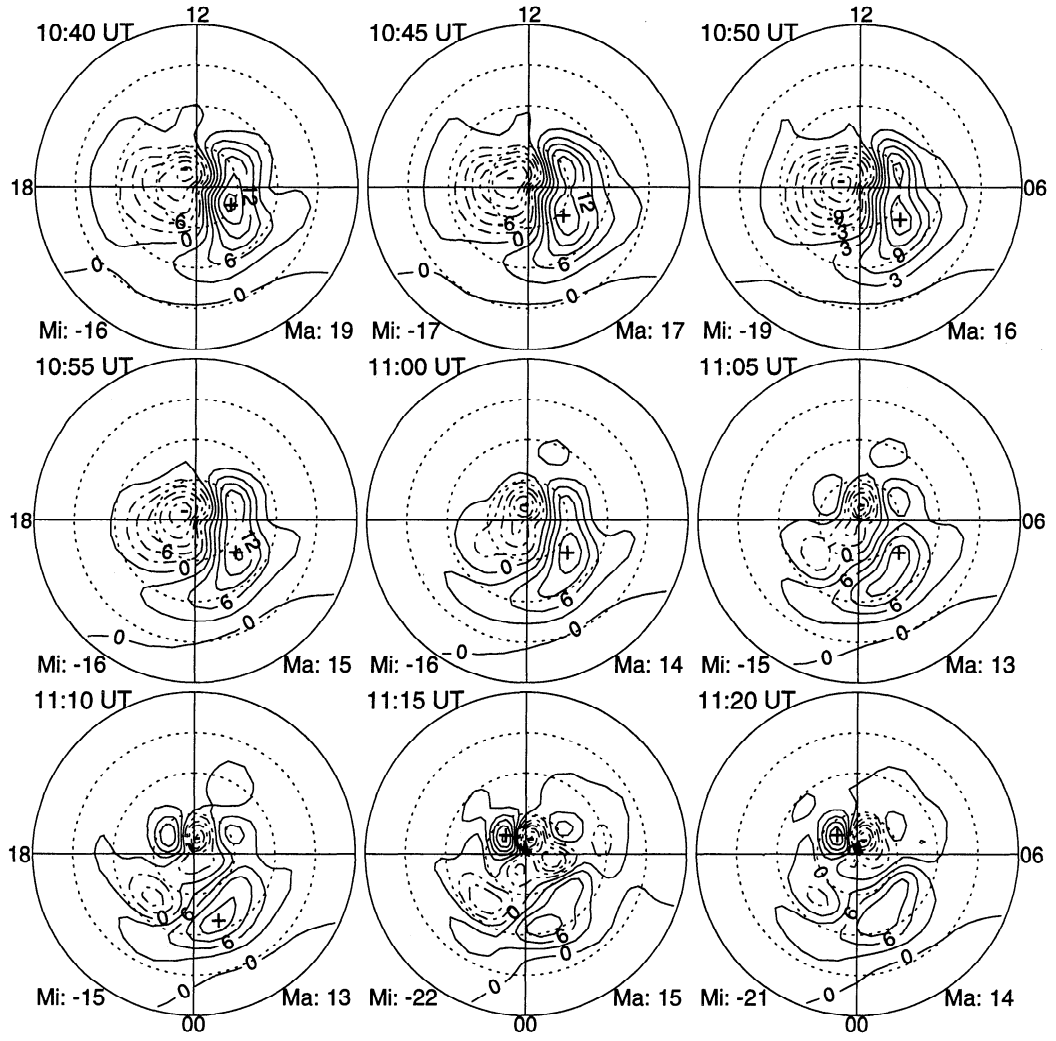

Figure 3. The 5-min ionospheric electric potential patterns for May 18, 1991, 1040 - 1120 UT. The data are displayed in polar magnetic coordinates, where the north magnetic pole is at the center, and the outer latitude is 50°. The top of each figure is magnetic local noon. The dashed contours represent negative potentials, while the solid contours represent positive potentials. The contour interval is 3 kV. The plus and minus signs show the location of the maximum and minimum potentials, respectively. "Mi" and "Ma" are the minimum and maximum potential, respectively.

the negative cell smaller in magnitude than the positive cell. The two cells do not appear to move, but remain at a fixed location, growing in strength with time.

The cross polar cap potential differences in the residual patterns (maximum potential change - minimum potential change) are plotted against time in Figure 5. The line plot can be easily divided into three intervals: (1) a nearly constant residual potential between 0 and 15 min; (2) a linear increase in the residual potential between 15 and 35 min; and (3) oscillating potentials around a constant residual potential value beyond 35 min. The dashed lines indicate the mean potential values during the first and third time intervals, while the dotted line indicates the linear increase in the residual potential. The start and stop times of the linear change are determined by using an iterative method, where the summed difference between the three fitted lines and the data points is minimized. The oscillations around the steady values may be due to uncertainties in the AMIE patterns. We estimate that the convection change took approximately 21 min, with a rate of change of 2.34 kV/min, for a total potential change of 49 kV (from 4 to 53 kV).

May 20, 1991

The second period of interest is on May 20, 1991. The IMF data for this period, as well as the location of the IMP 8 satellite, are shown in Figure 6. At approximately 1315 UT, the IMF B_y changes suddenly from 0 nT to -2 nT, where it remains nearly steady for 40 min. At 1400 UT, B_y starts decreasing slowly from -2 nT until it reaches a value of -5.5 nT at 1440 UT. At 1450 UT, B_y jumps from -5.5 nT to 4 nT in 3 min. During the entire period, B_z remains nearly steady at 6-8 nT. The changes in IMF orientation cause three convection changes to occur in the ionosphere.

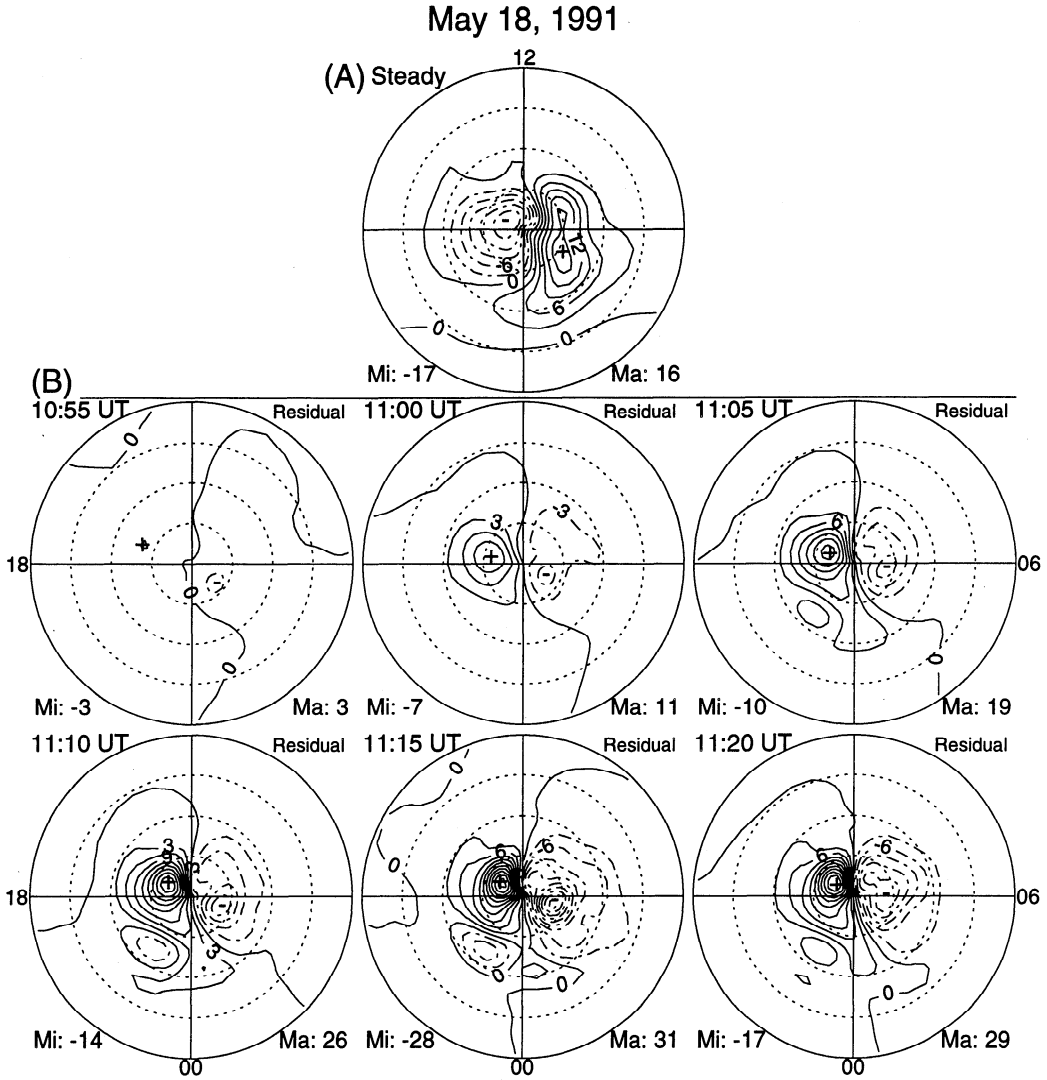

Figure 4. (a) The base pattern, displayed in the same fashion as Figure 3, is the average of the convection patterns between 1040 and 1055 UT. This pattern is considered to be the steady (base) potential pattern prior to the IMF reorientation. (b) The next six patterns show the residual potential, after subtracting the base pattern. The contours in these residual patterns represent the amount of potential added to or subtracted from an area. Solid contours indicate an increase in potential and negative contours represent a decrease in potential. The contour interval is 3 kV. The plus and minus signs represent location of the maximum positive and negative potential changes, respectively, while "Mi" and "Ma" indicate the minimum and maximum potential values.

A few representative convection patterns during the time period 1345 - 1545 UT are shown in Figure 7. At the start of this time period, there is a four-cell convection pattern, with two reversed convection cells located close to the pole, and two cells located on the nightside, which we attribute to viscous interaction. From 1345 UT to 1405 UT, the negative "reversed" cell fades. Then, from 1405 UT to 1420 UT, the positive "reversed" cell shrinks in spatial extent. These two convection changes are very small and hardly noticeable. The third convection change is very dramatic and starts at 1510 UT. The positive cell at the center of the polar cap begins to fade, while a negative cell emerges and becomes the dominant cell.

When a steady potential pattern (the 1335 UT and 1340 UT patterns, averaged together, shown in Figure 8a) is subtracted from the 1335 - 1445 UT patterns, a clear single cell can be seen to develop and intensify centered near the pole, on the noon-midnight meridian, toward noon. Three examples of these potential patterns are shown in Figure 8b. A weak negative cell develops at approximately 78° invariant latitude at 0900 MLT, but (throughout most of the period) is considerably weaker than the positive residual cell. The positive residual cell intensifies in its magnitude but with little spatial expansion, while the center of the cell remains in a fixed location.

Figure 9 shows the residual cross polar cap potential during this convection change. The dashed lines indicate steady time periods, while the dotted lines indicate the linear changes occurring in the ionospheric potential. One can see that there are two distinct changes.

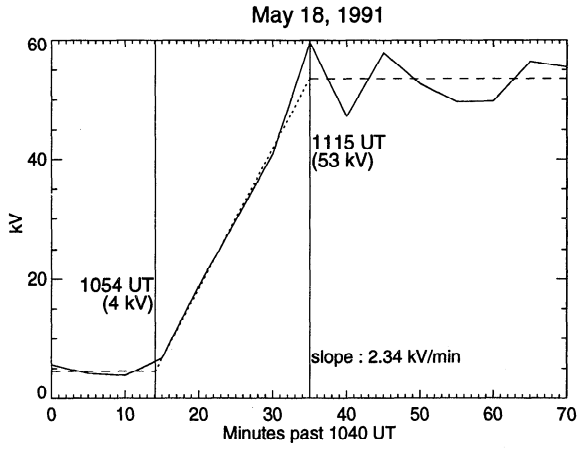

Figure 5. The cross polar cap potential difference of the residual potential patterns in Figure 4b versus time. Some additional times (not shown in Figure 4b) are used to expand the plot. The solid line shows the actual values derived from AMIE. The dashed lines show the steady state values, while the dotted line shows a linear progression between the two steady values (see text for additional information).

To verify this, a fit was done assuming only one change, and another was done assuming two changes. The minimum error in the least squares fit for two convection changes was less than half of the minimum error when only one convection change was assumed. Therefore, it is assumed that there were two changes. Starting at 1340 UT, a steep, almost linear, increase of 0.59 kV/min in the residual potential drop is observed. This increase lasts about 15 min. The potential then oscillates around a steady value of approximately 11 kV. At 1413 UT the potential begins to rise again. A second convection change of 8 kV occurs over a 13-min interval which gives a rate of change of 0.64 kV/min. These two convection changes were attributed to the first two IMF changes indicated in Figure 6.

For the third convection change, the convection patterns between 1440 and 1455 UT are averaged together (Figure 10a) and used as the base pattern. The residual patterns at 1510 UT, 1525 UT and 1545 UT are shown in Figure 10b. A single vortex structure can be seen to develop over the central polar cap, spreading much further toward midnight than noon, but with the largest potential change occurring near the pole. Once again, the residual potential patterns show that changes in the convection pattern are fixed in location; that is, the center of the residual cell remains at a fixed location. This change in the convection is attributed to the third IMF change indicated in Figure 6.

The potential change versus time is shown in Figure 11. The change again appears to be linear and occurs over approximately 24 min, with a potential change of 29 kV. The rate of change of this event is approximately 1.23 kV/min. It should also be noted that the IMF had a very sharp change, but the corresponding convection change took longer than the other events.

We attribute these three convection changes to the Y component of the IMF changing. Although B_x also changes (during the final IMF reorientation), we have not considered the ramifications of this change. It is observed that when B_y changes, but B_z is positive and large, the residual pattern is dominated by a single convection cell, centered nearly at the magnetic pole. The direction of the convection in this cell appears to be dependent on the sign of the B_y change. If the change in B_y is negative, the single residual plasma potential is positive; whereas if the change in B_y is positive, the residual cell is negative. The magnitude of the change in B_y determines the strength of the residual cell, as will also be shown later.

May 22, 1991

Figure 12 shows the IMF values and solar wind conditions for May 22, 1991, 0800 - 1100 UT, as well as the IMP 8 satellite position. There are two general changes occurring during this time period: (1) the solar wind number density changing from 50 to 4 particles/cm^3; and (2) the IMF magnitude increasing from 2 nT to 17

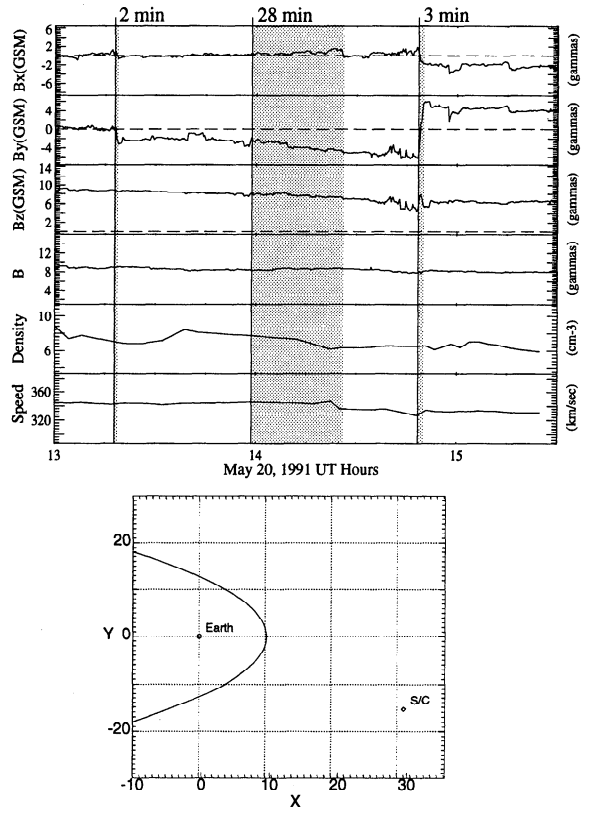

Figure 6. The interplanetary condition on May 20, 1991, from 1300 to 1530 UT, displayed in the same format as Figure 2. Note that there are three IMF changes during this period at 1320 UT, 1358 UT and 1450 UT, as indicated by the vertical lines. The time interval for each of the IMF orientation changes is noted at the top of the figure and is shaded. The first and last orientation changes are too short to have a significant grey area.

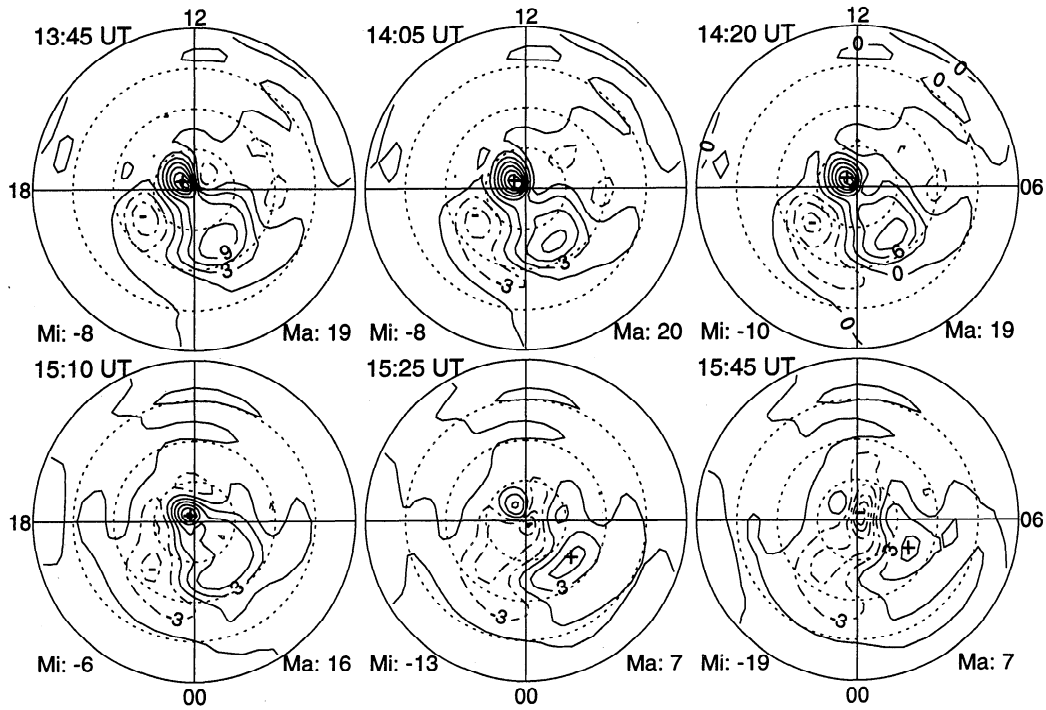

Figure 7. Ionospheric convection patterns from May 20, 1991, displayed in the same manner as Figure 3.

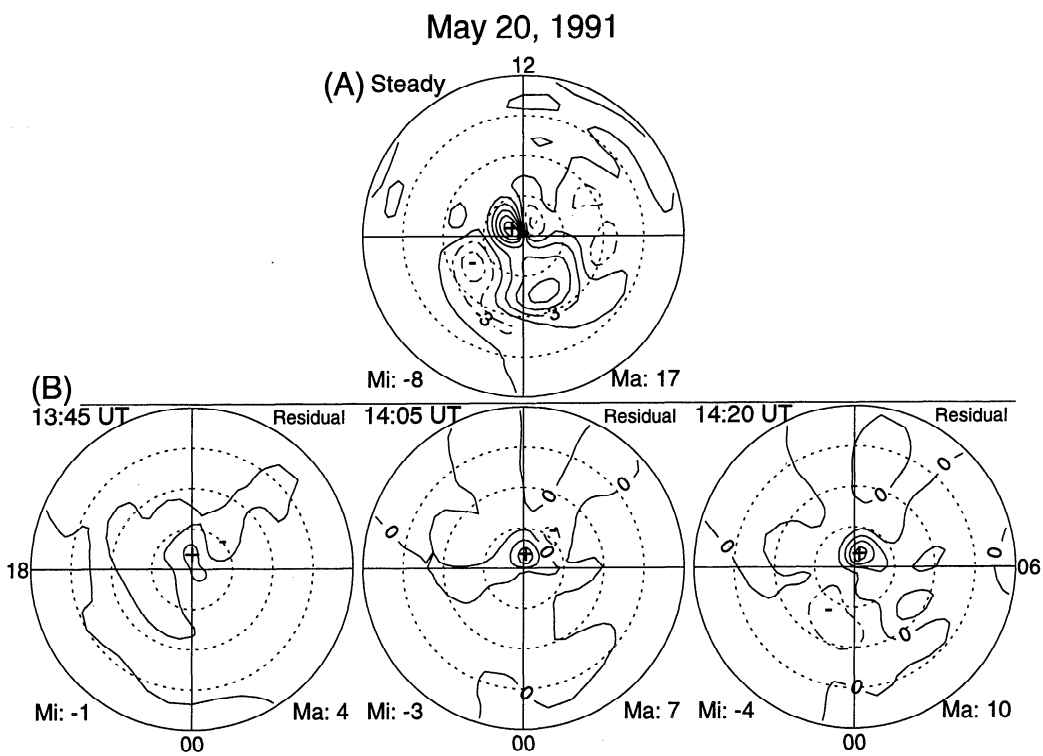

Figure 8. (a) The first potential pattern shows the steady pattern before the IMF reorientation. It is an average of the 1335 and 1340 UT potential patterns. (b) The residual patterns are shown in the same format as Figure 4.

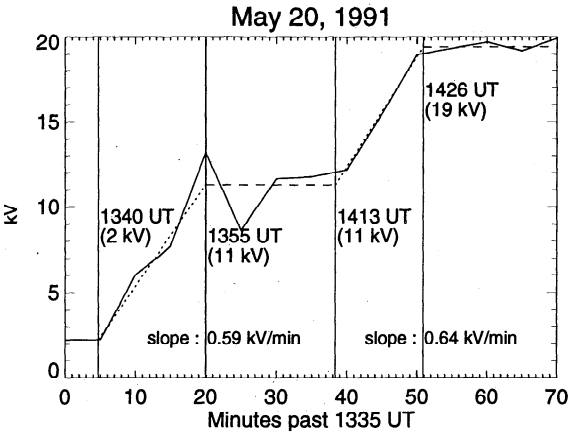

Figure 9. The cross polar cap potential difference of the residual potential patterns in Figure 8b shown in a manner similar to Figure 5. There are additional times included, which are not shown in Figure 8b, in order to expand the plot.

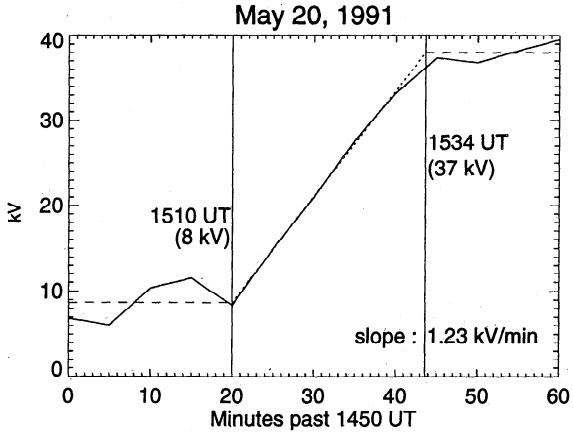

Figure 11. The cross polar cap potential difference of the residual potential patterns in Figure 10b shown in a manner similar to Figure 5. There are additional times included, which are not shown in Figure 10b, in order to expand the plot.

nT. The shaded areas highlight further fluctuations in the IMF: B_y rises from approximately 0 nT to 10 nT during the first shaded interval and then changes from 10 nT to -15 nT during the second interval; B_z increases from approximately 2 nT to 8 nT during the first interval and then changes from 8 nT to -5 nT in the second interval. In addition to the large-scale variations, there are smaller-scale variations in B_z.

The ionospheric convection patterns for the time period 0915 - 1025 UT are shown in Figure 13. During this time there are two distinct convection changes, although the first one is not as apparent as the second one. The first change starts at approximately 0935 UT and can be seen as the motion and intensification of the large negative cell in the afternoon region. Concurrent with this change is an increase in the magnitude of the positive cell located in the premidnight sector.

The steady state convection pattern is an average of the 0915 - 0925 UT patterns and is shown in Figure 14a. The convection change is more clearly observed in the

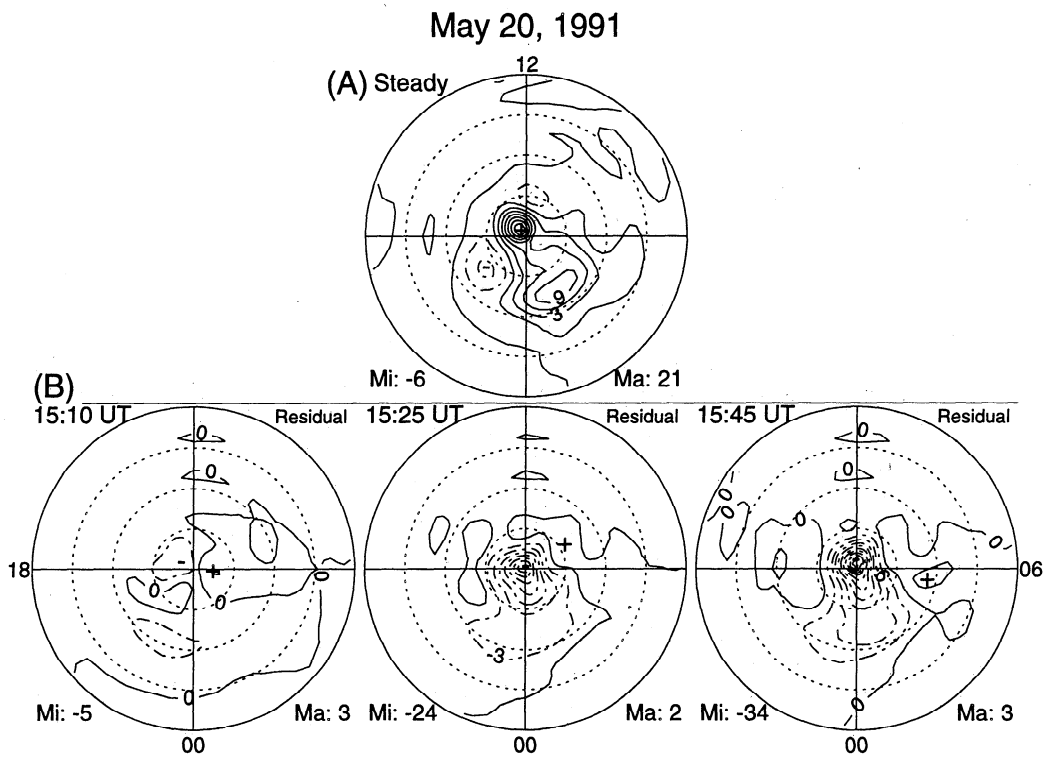

Figure 10. (a) The base pattern (an average of the 1440-1455 UT patterns) and (b) the residual potentials.

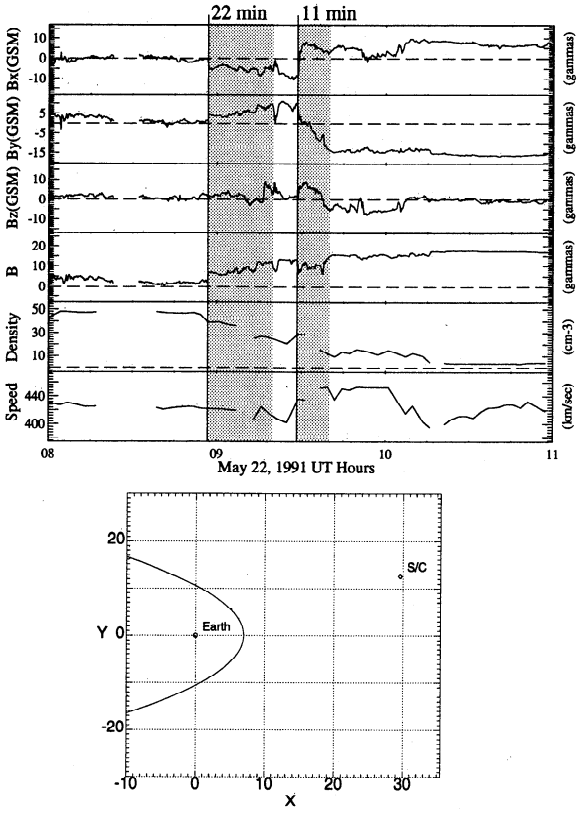

Figure 12. The IMF and solar wind conditions for May 22, 1991, 0800-1100 UT, displayed in the same manner as Figure 2. Note that there are two changes (0855 UT and 0928 UT) under investigation during this period, as indicated by the shaded time periods.

residual potentials, shown in Figure 14b. A negative cell is growing very close to the pole, while a positive cell is growing at 2200 MLT, at approximately 70° invariant latitude. These cells continue to grow until 0955 UT. The 0955 UT residual pattern is somewhat different from the previous one. The negative cell is being displaced from its previous position and has moved to 1500 MLT, implying that another convection change has started.

The residual potential change versus time is shown in Figure 15. The change takes approximately 19 min, and is approximately linear, with a total potential change of 31 kV, at a rate of 1.58 kV/min. The lack of a good fit to a linear change may be due in part to B_z fluctuations and also possibly to the variations observed in the solar wind density and speed. The automated fitting estimated the start time to be at 0933 UT, but it may be as early as 0925 UT, which would imply that the convection change may take as long as 27 min.

The second convection change in Figure 13 starts just after 0950 UT and appears to be a change from a narrowly confined convection pattern to a large two-cell convection pattern, typically driven by negative B_y and B_z. The cross polar cap potential drop also increases, which is indicative of a negative turning of B_z [*Reiff et al.*, 1981].

The base pattern is shown in Figure 16a. This is the last pattern of the previous change (0950 UT). This pattern must be used since there is not enough time delay between the changes to allow for averaging of two or more patterns. The residual patterns (Figure 16b) show no indication of the previous convection change (namely

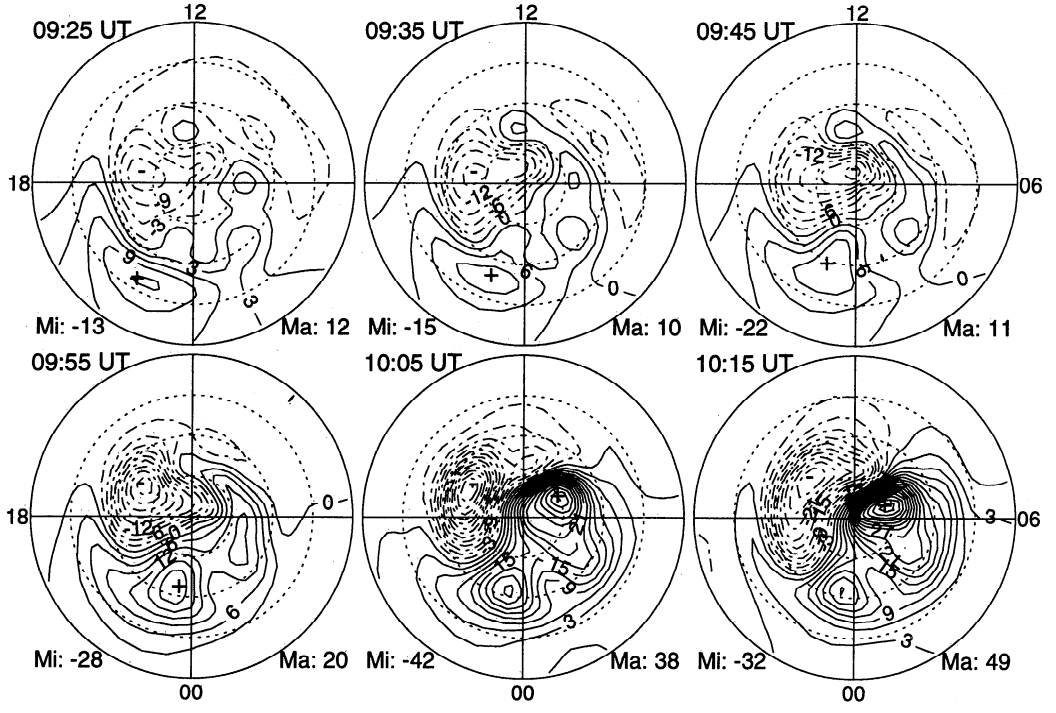

Figure 13. Potential patterns for May 22, 1991 displayed in the same manner as Figure 3.

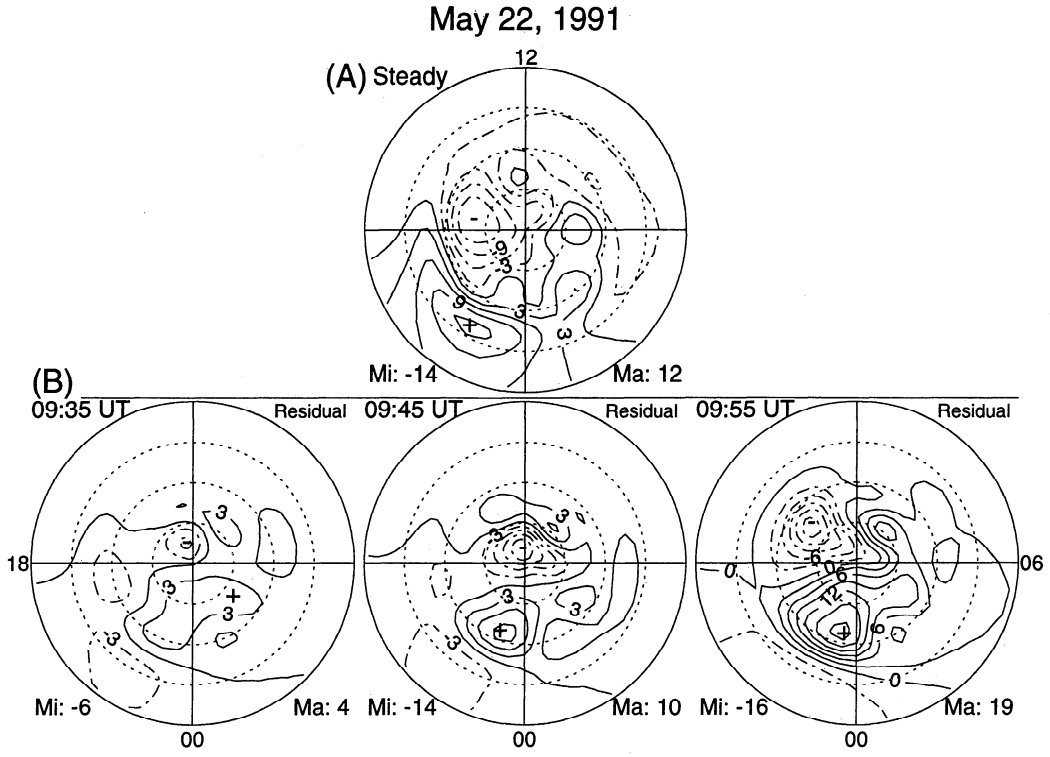

Figure 14. (a) The base pattern (an average of the 0915-0925 UT patterns) and (b) the residual potentials.

a residual positive potential near 2100 UT), while the 0950 UT residual potential pattern in Figure 16b shows no indication of the second convection change, so it appears that the convection changes did not overlap. In the residual potentials, there is a twin vortex structure which looks very much like a normal B_y negative, B_z negative convection pattern.

Figure 17 shows the residual potential drop against time. The convection change takes 15 min and appears to be linear once again. The rate of the potential change is 5.01 kV/min, the largest rate observed in this study.

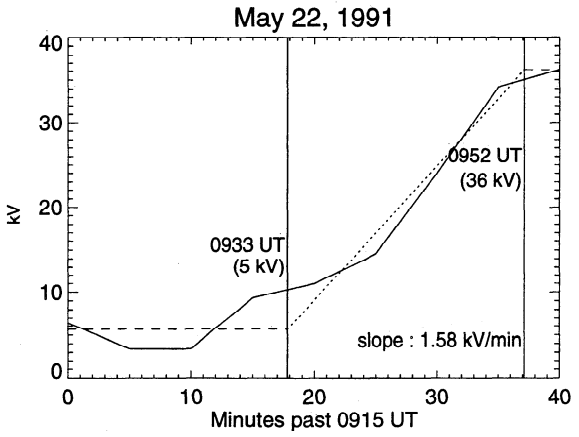

Figure 15. The cross polar cap potential difference of the residual potential patterns in Figure 14b versus time, displayed as in Figure 5. There are additional times used which are not shown in Figure 14b, in order to expand the plot.

Discussion

We have examined a total of six independent convection changes which can all be attributed to changes in the IMF. These convection changes all look different when a time series of ionospheric convection patterns is examined; but when a base pattern is subtracted, a number of similarities in the residual patterns start to emerge.

Development of Residual Potential Patterns

The first similarity is the lack of motion of the residual potential patterns. For all six convection changes, the residual potential cells seem to remain fixed at the same location and grow with time. This is quite different from the previous studies by *Saunders et al.* [1992], *Stauning et al.* [1995], and *Clauer et al.* [1995].

If the electric field of the IMF is applied across the ionospheric projection of the merging region first, and then slowly spreads out over the entire open field boundary, as proposed by *Saunders et al.* [1992], *Stauning et al.* [1995] and others, one would expect the convection pattern change to propagate away from the region where merging was initiated. However, we have shown that in all six events studied, the location and shape of the convection is constant, but the magnitude is changing.

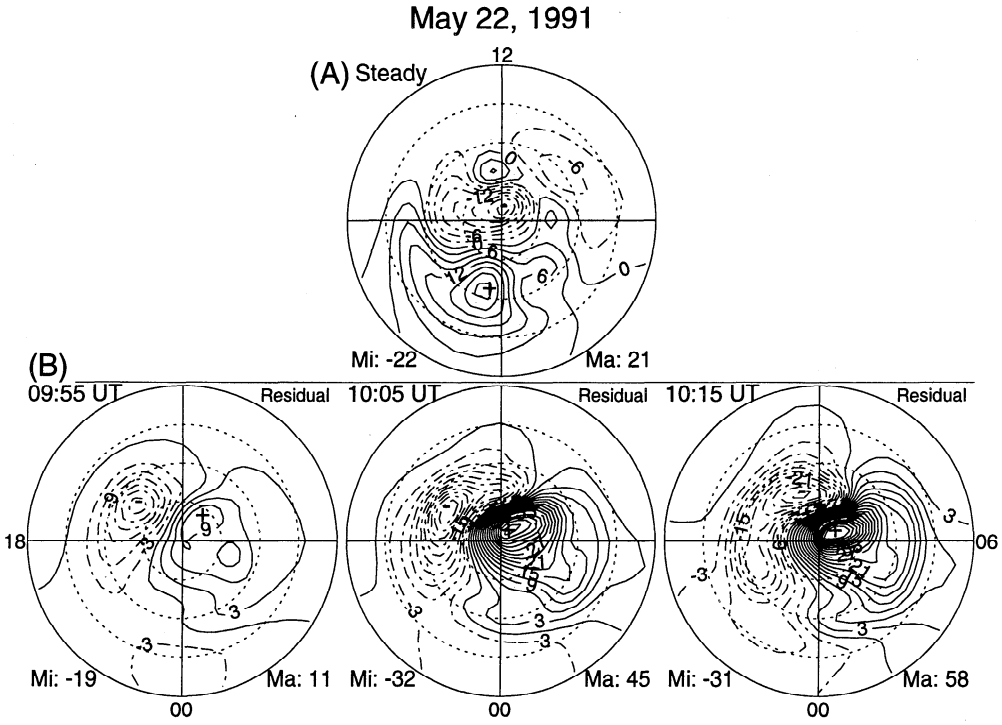

Figure 16. (a) The base pattern (the 0950 UT pattern) and (b) the residual potentials.

The idea of observing propagating phenomena during a convection change is not inconsistent with having residual potential patterns which are fixed in location but growing in magnitude. For example, Figure 13 shows many convection cells propagating: from 0935 UT to 0945 UT the minimum in the large negative potential cell moves from approximately 77° to 88°; from 0925 UT to 0955 UT the maximum in the positive potential cell is observed to move from 65° to 73°; from 0945 UT to 1005 UT the negative potential cell moves from the center of the polar cap to 75°. From these observations it seems to be obvious that the potential cells (and therefore field-aligned currents, electric field, etc.) are propagating with a measurable velocity. On the other hand, when the residual potential patterns are examined (Figures 14 and 16), one can see that the residual potential patterns are rather fixed in location, but with an intensification in the potential drop (also electric fields and field-aligned currents).

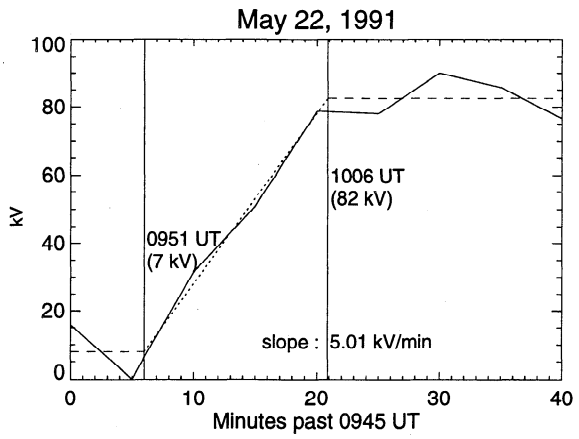

Figure 17. The cross polar cap potential difference of the residual potential patterns in Figure 16b versus time, displayed as in Figure 5. Additional times not shown in Figure 16b were used to expand the plot.

It is observed that there is no phase delay between dayside and nightside regions in the residual patterns, as one may otherwise infer from the original potential patterns. This lack of propagation can be explained if the electric field of the IMF is applied across the entire open field line boundary (i.e., the entire polar cap boundary) and is linearly increasing in strength. This is consistent with the superposition of the IMF electric field driven current systems discussed by *Banks et al.* [1984] and *Clauer and Banks* [1986].

One explanation for the rapid appearance of the electric field on the entire polar cap boundary is that the cross field line communication time in the ionosphere is fast compared to the Alfven wave travel time from the magnetopause to the ionosphere. This rapid communication may allow the ionospheric convection to reconfigure before magnetospheric regions away from the merging site reconfigure. This would imply that the electromotive force which is applied across the merging region is communicated quickly through out the ionosphere, and possibly back up to the magnetosphere.

Linear Convection Changes

The second similarity in the residual potential patterns appears when the residual cross polar cap potential drop is plotted out against time. For five of the six convection changes, a clear, linear change in residual potential is observed. These linear changes (as observed in Figures 5, 9, 11, and 17), along with the immobile residual patterns, imply that the electric field being applied to the ionosphere increases linearly with time.

Another way to describe the linear change is offered by *Parker* [1996]. He describes changing convection patterns as being caused by stresses which are being applied by the solar wind pulling the newly reconnected field lines toward the tail. This explanation, combined with the result which we have presented, would imply that this stress is steady in time and that the ionospheric plasma is being accelerated with a constant rate.

A linear relationship is also observed between the total residual potential change and the magnitude of the IMF changes (Figure 18a). The IMF magnitude changes were determined by taking the magnitude of the difference vector (before and after the change) in the GSM Y-Z plane. This shows that the potential change is linearly proportional to the magnitude of the IMF change (in the Y-Z plane), with a slope of 3.5 kV/nT.

A similar linear relationship between the IMF and the ionospheric potential has been observed before. *Papitashvili et al.* [1994], as described earlier, showed that the ground magnetic response is a linear function of the values of the Z and Y components of the IMF. If the IMF were to change from one orientation to another, one would expect that the change in the ground magnetic signatures would also be a linear function of the change in IMF. *Papitashvili et al.* [1994] determined the potential drop changes by approximately 4.5 kV/nT for B_y and 4.0 kV/nT for B_z changes (when B_z is positive). Although their study uses a different technique for deriving these relationships from this one, both show a linear character of the convection changes and obtain comparable proportionality factors.

Figure 18b shows the rate of change of the ionospheric potential pattern (the slope of the linear changes in Figures 5, 9, etc.) versus the magnitude of the IMF orientation change (as described above). The correlation is once again linear, with a slope of 0.2 $\mathrm{kVmin^{-1}nT^{-1}}$, showing that the reconfiguration of the ionosphere occurs at a faster rate for stronger IMF changes. This would imply that a larger stress is applied across the ionosphere for larger changes in IMF orientation, thereby accelerating the plasma at a faster rate. Similarly, one could describe the rate of the application of the interplanetary electric field as being linearly dependent on the magnitude of the IMF reorientation.

Shape of the Residual Patterns

We show four examples of changing convection patterns which we associate with changes in the Y component of the IMF: the three events on May 20 and the first event on May 22. All of these events show a single residual potential cell located at approximately magnetic pole. The sign of the residual potential cell is determined by the sign of the change in B_y: For positive (negative) changes in B_y, the residual potential cell is negative (positive).

One would expect that an increase in the magnitude of B_y would cause the merging region to move further away from the noon-midnight meridian [e.g., *Crooker*, 1979], thereby causing the tension in the newly merged field lines to increase. This increased tension in the dawn-dusk direction would cause more dawn-dusk motion of the field lines. The fact that residual patterns associated with a changing B_y show only east or west flow along the noon-midnight meridian indicates that there is a change in the tension in the dawn-dusk direction.

For example, in the case in which B_y completely changes sign (May 20, 1991 at 1450 UT), the direction of

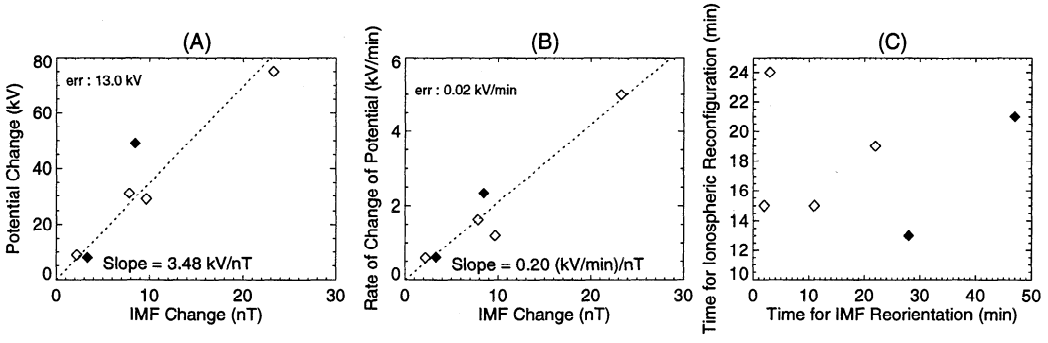

Figure 18. (a) The final, steady, cross polar cap potential difference of the residual potential patterns, versus the magnitude of the IMF reorientation in the Y-Z plane. (b) The rate of change of the cross polar cap potential difference of the residual potential patterns, versus the magnitude of the IMF reorientation in the Y-Z plane. (c) The time for the ionospheric reconfiguration, versus the time for the IMF reorientation. A linear relationship is observed in the first two plots. However, there is no clear correlation in the third. The solid data points indicate events in which the IMF takes longer to reorient than the ionosphere takes to reconfigure.

the flow (associated with the dayside merging) reverses (Figure 7), and a large negative residual potential cell forms (Figure 10). This is consistent with the tension in the magnetic field lines changing from duskward to dawnward, with a net tension change in the dawnward direction.

Reconfiguration Times

Figure 18c shows the ionospheric reconfiguration times (IRTs) against the IMF reorientation times. The IRT is derived from the residual cross polar cap potential drop versus time plots (see Figures 5, 9, 11, 15, and 17), while the IMF reorientation times are indicated by the shaded intervals in Figures 2, 6, and 12. A lower limit of 12 min and an upper limit of 24 min for the IRT are observed. Besides these lower and upper limits, there appears to be no clear correlation to the data.

For sudden changes in IMF orientation, we would expect that the IRT has little correlation with the amount of time the IMF takes to change [*Hairston and Heelis*, 1995; *Etemadi et al.*, 1988; *Clauer and Friis-Christensen*, 1988]. On the other hand, for IMF reorientations which take much longer than the Alfven travel time between the magnetopause and the ionosphere, we would expect there to be some correlation between the IMF reorientation time and the IRT. For example, *Cumnock et al.* [1992] and *Knipp et al.* [1993] studied a time period in which a magnetic cloud is encountering the magnetosphere and the IMF is rotating very slowly. They show that the ionospheric convection pattern is developing over a similar timescale as the IMF reorientation.

For our study we present two IMF reorientations (May 18 at 1100 UT and May 20 at 1400 UT) which take longer than the corresponding ionospheric reorientations. These two events are highlighted in Figure 18 to show that they are different than the rest of the events. By examining these long-duration IMF reorientations (longer than a few minutes, but less than many hours) we may gain some insight into the dynamics of the merging region on the dayside magnetopause.

It is well known that for a northward oriented IMF, the ratio $B_z/|B_y|$ determines whether the ionospheric convection will be reversed or not [*Taguchi et al.*, 1993; *Cumnock et al.*, 1995; *Papitashvili et al.*, 1995]. We speculate that there may be a similar type of thresholding between the IMF and the magnetosphere for the long-duration IMF orientation changes. We define θ to be the angle between B_z and $|B_y|$, such that

$$\theta = \tan^{-1}\left(\frac{B_z}{|B_y|}\right). \quad (1)$$

We speculate that the merging region may not begin to change until $|\Delta\theta|$ becomes larger than some value. The first IMF reorientation which took longer than the corresponding ionospheric reconfiguration (on May 18) is from $B_z/|B_y| = 0$ to $B_z/|B_y| \cong 2$, or $\theta = 0°$ to $\theta = 60°$, a $\Delta\theta$ of 60°. The second change (May 20, at 1400 UT) is from $B_z/|B_y| = 4.3$ ($\theta = 77°$) to $B_z/|B_y| = 1.4$ ($\theta = 54°$), a $\Delta\theta$ of $-23°$.

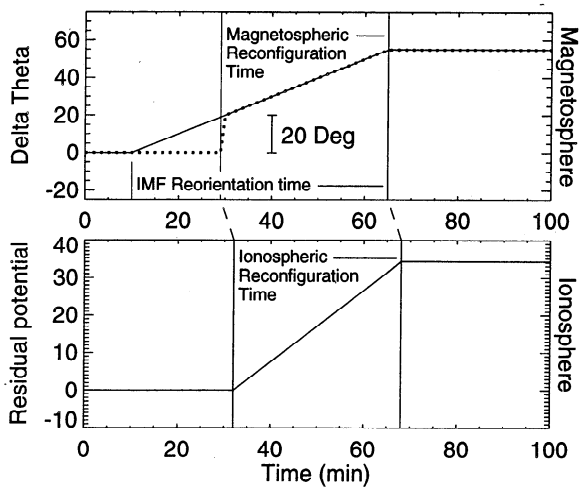

Figure 19. A hypothetical change in the IMF and the corresponding reaction in the (top) magnetosphere and (bottom) ionosphere. The magnetospheric reaction is shown as a dotted line, while the IMF is shown as a solid line.

To further illustrate this point, Figure 19 shows a hypothetical IMF orientation change, as well as the corresponding response of the ionospheric residual cross polar cap potential. It is assumed that the magnetosphere does not start to react to the change in the IMF until $\Delta\theta$ has reached a value of 20°. At this time, the magnetosphere reacts as if there was a sudden change followed by a slower change in the IMF. Therefore the magnetosphere reacts to the full magnitude change in the IMF, but with a shorter reconfiguration time than the IMF reorientation time. The ionosphere begins to react a few minutes later than the magnetosphere. The inductive effects of the magnetosphere - ionosphere system may cause the steep and gradual change in the magnetosphere to be a single gradual change in the ionosphere.

We have only examined two changes in which the ionospheric reconfiguration time was shorter than the corresponding IMF orientation time. Because of this, the value of $\Delta\theta$ which triggers the change in the magnetosphere is unknown. This quantity may be fixed, but it may be highly dependent on a number of different parameters such as the solar wind and the history of IMF orientation.

Limitations

Although we have presented new ideas on how the solar wind and interplanetary magnetic field control convection in the ionosphere, only six examples have been presented in this paper. It is obvious that more case studies are needed in order to make a more definitive conclusion.

Many of the previous studies [e.g., *Saunders et al.*, 1992; *Stauning et al.*, 1995; *Clauer et al.*, 1995] focus on events which occurred when the IMF B_z was southward or when the B_z or B_y component was oscillating. For most of the events presented in this paper, the IMF was directed northward, so the convection was confined

to a very small region. Further studies are needed for southward IMF orientations to determine if the ionospheric convection responds in the same manner as we have observed in this paper.

Conclusions

We show a number of cases in which the ionospheric convection underwent a change from one configuration to another. When a base potential pattern, obtained immediately before the change, is subtracted from the rest of the patterns, the residual patterns show more clearly how the ionosphere responds to the IMF changes. By examining these residual convection patterns, we have reached the following conclusions:

1. The ionospheric convection changes seem to remain in the same position, having approximately the same shape, but increase in strength with time. This result is quite different from (but not inconsistent with) previous interpretations based only on localized observations, which showed the convection change propagating away from the dayside merging region [e.g., *Saunders et al.*, 1992; *Stauning et al.*, 1995; *Clauer et al.*, 1995].

The analysis here shows that there is no propagation of the changing convection cells away from the cusp region, as was previously speculated, and that the penetrating electric field is being applied across the entire polar cap boundary on a very rapid timescale (a few seconds). This electric field in the ionosphere is increasing in magnitude with time. The present study mainly focuses on convection changes which occur while B_z is positive, while past studies have focused mainly on either B_z changes or B_y changes with negative B_z.

2. Ionospheric convection changes are approximately linear. For all cases that we have studied in this paper, the residual potential drop increases lincarly with time. We may assume then that the immobile ionospheric electric field is increasing linearly with time. This can also be described as a stress being applied across the ionosphere which causes the ionospheric plasma to accelerate across the polar cap [e.g. *Parker*, 1996].

3. The potential change which occurs in the ionosphere is linearly dependent upon the magnitude of the IMF reorientation in the $Y-Z$ plane. Many papers have shown that the cross polar cap potential is related to the magnitude of the IMF Y and Z components [e.g., *Reiff et al.*, 1981; *Papitashvili et al.*, 1994]. The proportionality factor which we have derived (3.5 kV/nT) is similar to the values derived by *Papitashvili et al.* [1994] (4.5 kV/nT for B_y and 4.0 kV/nT for positive B_z.)

4. The rate of change of the residual cross polar cap potential drop is linearly dependent on the magnitude of the IMF orientation change in the Y-Z plane, with a proportionality factor of 0.2 $\mathrm{kVmin^{-1}nT^{-1}}$.

5. The shape of the residual potential cells is strongly dependent on the IMF orientation before and after the change. We have shown that when B_z is positive and B_y changes, the dayside residual potential will be a single narrowly confined cell, either a positive potential cell (counterclockwise plasma flow) for decreases in B_y or a negative potential cell (clockwise plasma flow) for increases in B_y.

6. The amount of time that the ionosphere takes to reconfigure, after a change in IMF orientation, is between 12 and 24 min, if the IMF change takes 50 min or less time. We speculate that some IMF reorientations may actually take longer than the corresponding ionospheric reconfiguration time, because the merging region may not change until the ratio of the IMF components reaches, or passes through, a certain threshold. But the magnetosphere is likely to react to the entire change in the IMF. We have not examined changes which take longer than 50 min, so we can not speculate on the ionospheric reconfiguration times for these changes.

Although we have discussed a number of different aspects of the solar-wind - magnetospheric - ionospheric interactions, we have only examined six cases. We feel that more studies, similar to this, will be needed in order to reinforce some of the ideas presented in this paper.

Acknowledgments. The data used for this study are provided by a number of different sources. Table 1 lists all of the magnetometers which were used in this study, along with the network from which the magnetometer came from. The Greenland magnetometer data were supplied by Eigil Friis-Christensen at the Danish Meteorological Institute. The CANOPUS instrument array was constructed and is maintained and operated by the Canadian Space Agency. The International Monitor for Auroral Geomagnetic Effects (IMAGE) is a joint European project for establishing and maintaining a network of digital magnetometers from southern Finland to the northern part of Svalbaard (H. Lühr, Institute for Geophysics and Meteorology, Germany, and L. Hakkinen, Finnish Meteorological Institute). The SAMNET magnetometer data were supplied by Marc Lester at the Department of Physics and Astronomy, University of Leicester. The Norway magnetometer data were supplied by the Auroral Observatory of Tromso. The Intermagnet magnetometer data are available via CD-ROM and are supplied by the National Geomagnetic Information Center, U.S. Geological Survey (Golden, Colorado). The NGDC magnetometer data were supplied by Leslie Morris at the World Data Center. DMSP particle, drift meter and hemispheric power index data were provided by Fred Rich at Phillips Laboratory on Hanscom Air Force Base. David Evans supplied hemispheric power indices from the NOAA 12 satellite. The IMP 8 magnetic field data have been provided by Ron Lepping at NASA Goddard, and the plasma data have been provided by Alan Lazarus at MIT. The Sondrestrom upper atmospheric research facility in Kangerlussuaq, Greenland, is managed and operated jointly for the National Science Foundation (NSF) and the Danish Meteorological Institute by SRI International. We would like to thank Art Richmond for his insightful thoughts. This work has been supported at the University of Michigan by NSF grants ATM-9412390, ATM-9501380, and OPP-9318766 and at the High Altitude Observatory (HAO) by NSF grant SA93-SFA.1. One of the authors (AJR) was supported by a Newkirk Fellowship at HAO.

The Editor thanks J.D. Menietti and D.W. Lennartsson for their assistance in evaluating this paper.

References

Abston, C.C., N.E. Papitashvili, and V.O. Papitashvili, Combined International Catalog of Geomagnetic Data, *Rep. UAG-92, WDC-A for STP, WDC-B2 and WDC-C*, Natl. Geophys. and Sol.-Terr. Data Cent., Natl. Oceanic and Atmos. Admin., Boulder, Colo., 1985.

Banks, P.M., T. Araki, C.R. Clauer, J.P. St. Maurice, and J.C. Foster, The interplanetary magnetic field, cleft currents, and plasma convection in the polar caps, *Planet. Space Sci.*, *32*, 1551, 1984.

Belov, B.A., R.G. Afonina, A.E. Levitin, and Y.I. Feldstein, The effects of interplanetary magnetic field orientation on geomagnetic field at the nothern polar cap, in *Variations of Magnetic Field and the Aurora*, edited by Y.I. Feldstein and A.E. Levitin, *p. 15*, Izmiran, Moscow, 1977.

Cannon, P.S., G. Crowley, B.W. Reinisch, and J. Buchau, Digisonde measurements of polar cap convection for northward interplanetary magnetic field, *J. Geophys. Res.*, *97*, 16877, 1992.

Clauer, C.R. and P.M. Banks, Relationship of the interplanetary electric field to the high-latitude ionospheric electric field and currents: Observations and model simulation, *J. Geophys. Res.*, *91*, 6959, 1986.

Clauer, C.R. and E. Friis-Christensen, High-latitude dayside electric field and currents during strong northward interplanetary magnetic field: Observations and model simulation, *J. Geophys. Res.*, *93*, 2749, 1988.

Clauer, C.R., P. Stauning, T.J. Rosenberg, E. Friis-Christensen, P.M. Miller, and R.J. Sitar, Observations of a solar-wind-driven modulation of the dayside ionospheric DPY current system, *J. Geophys. Res.*, *100*, 7697, 1995.

Crooker, N.U., Dayside merging and cusp geometry, *J. Geophys. Res.*, *84*, 951, 1979.

Crooker, N.U., Reversed convection, *J. Geophys. Res.*, *97*, 19363, 1992.

Cumnock, J.A., R.A. Heelis, and M.R. Hairston, Response of the ionospheric convection pattern to a rotation of the interplanetary magnetic field on January 14, 1988, *J. Geophys. Res.*, *97*, 19449, 1992.

Cumnock, J.A., R.A. Heelis, M.R. Hairston, and P.T. Newell, High-latitude ionospheric convection pattern during steady northward interplanetary magnetic field, *J. Geophys. Res.*, *100*, 14537, 1995.

Dungey, J.W., Interplanetary magnetic field and the auroral zones, *Phys. Rev. Lett.*, *93*, 47, 1961.

Etemadi, A., S.W.H. Cowley, M. Lockwood, B.J.I. Bromage, D.M. Willis, and H. Lühr, The dependence of high-latitude dayside ionospheric flows on the north-south component of the IMF: A high time resolution correlation analysis using Eiscat "POLAR" and AMPTE UKS and IRM data, *Planet. Space Sci.*, *36*(5), 471, 1988.

Feldstein, Y.I. and A.E. Levitin, Solar wind control of electric fields and currents in the ionosphere, *J. Geomagn. Geoelectr.*, *38*, 1143, 1986.

Foster, J.C., An empirical electric field model derived from Chatanika radar data, *J. Geophys. Res.*, *88*, 981, 1983.

Friis-Christensen, E. and J. Wilhjelm, Polar cap currents for different directions of the interplanetary magnetic field in the $Y-Z$ plane, *J. Geophys. Res.*, *80*, 1248, 1975.

Friis-Christensen, E., Y. Kamide, A.D. Richmond, and S. Matsushita, Interplanetary magnetic field control of high-latitude electric fields and currents determined from Greenland magnetometer chain, *J. Geophys. Res.*, *90*, 1325, 1985.

Greenwald, R.A., K.B. Baker, J.M. Ruohoniemi, J.R. Dudeney, M. Pinnock, N. Mattin, J.M. Leonard, and R.P. Lepping, Simultaneous conjugate observations of dynamic variations in high-latitude dayside convection due to changes in IMF B_y, *J. Geophys. Res.*, *95*, 8057, 1990.

Hairston, M.R. and R.A. Heelis, Response time of the polar ionospheric convection pattern to changes in the north-south direction of the IMF, *Geophys. Res. Lett.*, *22*, 631, 1995.

Heelis, R.A., The effects of interplanetary orientation on dayside high-latitude convection, *J. Geophys. Res.*, *89*, 2873, 1984.

Heppner, J.P. and N.C. Maynard, Empirical high-latitude electric field models, *J. Geophys. Res.*, *92*, 4467, 1987.

Holt, J.M., R.A. Wand, J.V. Evans, and W.L. Oliver, Empirical models for the plasma convection at high latitudes from Millstone Hill observatory, *J. Geophys. Res.*, *92*, 203, 1987.

Knipp, D.J., A.D. Richmond, B. Emery, N.U. Crooker, O. de la Beaujardière, D.S. Evans, and H.W. Kroehl, Ionospheric convection responce to changing IMF direction, *Geophys. Res. Lett.*, *18*, 721, 1991.

Knipp, D.J. et al., Ionospheric convection response to slow, strong variations in a northward interplanetary magnetic field: A case study for January 14, 1988, *J. Geophys. Res.*, *98*, 19273, 1993.

Lester, M., O. de la Beaujardière, J.C. Foster, M.P. Freeman, H. Lühr, J.M. Ruohoniemi, and W. Swider, The responce of the large scale ionospheric convection pattern to changes in the IMF and substorms: Results from the SUNDIAL 1987 campaign, *Ann. Geophys.*, *11*, 556, 1993.

Levitin, A.E., R.G. Afonina, B.A. Belov, and Y.I. Feldstein, Geomagnetic variation and field-aligned currents at northern high-latitudes, and their relations to the solar wind parameters, *Philos. Trans. R. Soc. London, Ser. A*, *304*, 253, 1982.

Lockwood, M., S.W.H. Cowley, and M.P. Freeman, The excitation of plasma convection in the high-latitude ionosphere, *J. Geophys. Res.*, *95*, 7961, 1990.

Lu, G. et al., Interhemispheric asymmetry of the high-latitude ionospheric convection pattern, *J. Geophys. Res.*, *99*, 6491, 1994.

Maczawa, K., Magnetic convection induced by the positive and negative z-components of the interplanetary magnetic field: Quantitative analysis using polar cap magnetic records, *J. Geophys. Res.*, *81*, 2289, 1976.

Papitashvili, V.O., B.A. Belov, D.S. Faermark, Y.I. Feldstein, S.A. Golyshev, L.I. Gromova, and A.E. Levitin, Electric potential patterns in the northern and southern polar regions parameterized by the interplanetary magnatic field, *J. Geophys. Res.*, *99*, 13251, 1994.

Papitashvili, V.O., C.R. Clauer, A.E. Levitin, and B.A. Belov, Relationship between the observed and modeled modulation of the dayside ionospheric convection by the IMF B_y component, *J. Geophys. Res.*, *100*, 7715, 1995.

Parker, E.N., The alternate paradigm for magnetospheric physics, *J. Geophys. Res.*, *101*, 11000, 1996.

Reiff, P.H., Sunward convection in both polar caps, *J. Geophys. Res.*, *87*, 5976, 1982.

Reiff, P.H., R.W. Spiro, and T.W. Hill, Dependence of polar cap potential on interplanetary parameters, *J. Geophys. Res.*, *86*, 7639, 1981.

Rich, F.J. and M. Hairston, Large-scale convection patterns observed by DMSP, *J. Geophys. Res.*, *99*, 3827, 1994.

Richmond, A.D., Ionospheric electrodynamics using magnetic apex coordinates, *J. Geomagn. Geoelectr.*, *47*, 191, 1995.

Richmond, A.D. and Y. Kamide, Mapping electrodynamic features of the high-latitude ionosphere from localized observations: Technique, *J. Geophys. Res.*, *93*, 5741, 1988.

Ridley, A.J. and C.R. Clauer, Characterization of the dynamic variations of the dayside high-latitude ionospheric convection reversal boundary and relationship to interplanetary magnetic field orientation, *J. Geophys. Res.*, *101*, 10919, 1996.

Ruohoniemi, J.M. and R.A. Greenwald, Statistical patterns of the high-latitude convection obtained from Goose Bay HF radar observations, *J. Geophys. Res.*, *101*, 21743, 1996.

Saunders, M.A., M.P. Freeman, D.J. Southwood, S.W.H. Cowley, M. Lockwood, J.C. Samson, C.J. Farrugia, and T.J. Hughes, Dayside ionospheric convection changes in response to long-period interplanetary magnetic field oscillations: Determination of the ionospheric phase velocity, *J. Geophys. Res.*, *97*, 19373, 1992.

Senior, C., D. Fontaine, G. Caudal, D. Alcaydé, and J. Fontanari, Convection electric fields and electrostatic potential over $61^\circ < \lambda < 72^\circ$ invariant latitude observed with the European incoherent scatter facility, 2, Statistical results, *Ann. Geophys.*, *8*, 257, 1990.

Stauning, P., C.R. Clauer, T.J. Rosenberg, E. Friis-Christensen, and R. Sitar, Observations of solar-wind-driven progression of interplanetary magnetic field B_y-related dayside ionospheric disturbances, *J. Geophys. Res.*, *100*, 7567, 1995.

Taguchi, S., M. Sugiura, J.D. Winningham, and J.A. Slavin, Characterization of the IMF B_y-dependent field-aligned currents in the cleft region based on DE 2 observations, *J. Geophys. Res.*, *98*, 1393, 1993.

Weimer, D.R., Models of high-latitude electric potentials derived with a least error fit of spherical harmonic coefficients, *J. Geophys. Res.*, *100*, 19595, 1995.

C. R. Clauer and V.O. Papitashvili, Space Physics Research Laboratory, University of Michigan, Ann Arbor, MI 48109.

G.Lu and A.R. Ridley, High Altitude Observatory, National Center for Atmospheric Research, P.O. Box 3000, Boulder, CO 80307. (e-mail: ridleya@hao.ucar.edu)

(Received November 5, 1996; revised March 3, 1997; accepted March 26, 1997.)